An Experimental Study of the Low-Lying Electronic States of WO_2

Gustavo E. Davico, Rebecca L. Schwartz, Tanya M. Ramond, and W. Carl Lineberger*

JILA, University of Colorado and National Institute of Standards and Technology, and Department of Chemistry and Biochemistry, University of Colorado, Boulder, Colorado 80309-0440

Received: April 8, 1999; In Final Form: June 7, 1999

The 364 nm negative ion photoelectron spectrum of WO_2^- is obtained. The spectrum reveals that four different electronic states are accessed in the neutral molecule following electron detachment. From the rich vibrational structure the vibrational frequencies of the bending and/or symmetric stretching vibrations are measured. The electron affinity is determined to be $1.998(10) - 0.040k$ eV, where $k = 0$, 1, or 2. Theoretical calculations have been carried out to determine the geometries, energies, and frequencies of the anion and neutral molecules. These are utilized to generate a simulation of the experimental spectrum. The excellent agreement between the spectrum and the simulation indicates that the changes in geometries upon detachment are well predicted by the theoretical method employed, at least for the two lowest electronic states. In addition, polarization studies enable us to determine the asymmetry parameters for each state and thus confirm the assignments of the electronic states.

Introduction

The properties of metal oxides such as tungsten dioxide (WO_2), in addition to their high melting point, which makes them well-suited for high-temperature applications, exhibit great potential for industrial interests. For example, the structure of WO_2 departs from the regular rutile structure characterized by TiO_2 and many other transition metal oxides. This distorted structure allows the formation of metal−metal bonding, which changes the band structure and therefore the electrical conductivity properties.[1−4] Transition metal oxides, including tungsten oxides, are relevant to solar energy technology. Films of tungsten oxides produced by chemical vapor deposition demonstrate that they have a high solar absorbance, which is critical to the efficient conversion of solar energy to heat.[5] One of the most common applications of transition metal oxides is as catalysts in the selective oxidation of organic substrates.[6] Tungsten oxides, like the related chromium and molybdenum oxides, have been used as selective catalysts for a variety of oxidation reactions.[7] There is evidence that the reaction proceeds through a mechanism that involves the formation of a tungsten peroxo compound.[7−9] The Fermi density of states observed in solid WO_2 by using X-ray photoelectron spectroscopy has been identified as the cause of its catalytic properties in the hydrogenolysis of organic compounds.[4]

Despite the need to understand the macroscopic and catalytic properties of WO_2, little is known of its structure in noncrystalline form. What is known comes from studies that have obtained the vibrational frequencies of WO_2 in rare gas matrixes.[10−12] In early experiments, Weltner and McLeod[12] examined the spectra of WO_2 in a neon matrix in both the visible and infrared regions. They were able to measure the frequencies of all three vibrational modes: the symmetric stretch (ν_1), the bend (ν_2), and the antisymmetric stretch (ν_3). Similarly, Green and Ervin[10] obtained infrared spectra of three WO_2 isotopomers in krypton matrixes, from which they were able to measure the stretching frequencies. In addition, from their measured frequencies, and assuming a harmonic oscillator approximation, they calculated an upper limit to the O−W−O bond angle, 119°. Taking into account the anharmonicity of the vibration, they refined this value to be 114°. Values for the symmetric and antisymmetric stretching frequencies in WO_2 were also measured in methane matrixes.[9] More recently, Andrews and co-workers[11] have recorded the infrared spectrum of WO_2 in an argon matrix, enabling them to obtain values for the symmetric and antisymmetric stretching frequencies. From these data, they calculated an average value of 124° for the O−W−O bond angle. All of the above-mentioned experimental studies illustrate that the WO_2 molecule has a bent geometry in the ground electronic state.

Negative-ion photoelectron spectroscopy provides a method[13] by which spectral information can be gained, such as electronic state information that was inaccessible through the matrix spectroscopy studies. Because of mass-selection capabilities, there is no complication in the assignments due to the presence of other tungsten oxide species produced simultaneously with WO_2, as was found in the matrix isolation methods. By using 3.408 eV photons, we can probe many of the low-lying electronic states common to metal oxides, as well as their corresponding vibrational levels.

In this paper we describe the photoelectron spectrum of WO_2^-. The lowest four electronic states of WO_2 are accessed following electron detachment. Results of ab initio calculations are presented; they aid in assigning the various peaks in the spectrum and in labeling the electronic states. Experimental frequencies for the symmetric stretching and bending vibrations are reported and compared with the calculated values. Previous theoretical and experimental studies on WO_2 have resulted in vibrational frequencies for only one electronic state. Comparisons with these values are made when appropriate. Simulations derived from our calculations are presented and discussed.

Experiment

The details of the photoelectron spectrometer are described elsewhere;[13] only a brief overview is given here. WO_2^-, along

* Corresponding author. E-mail: WCL@JILA.COLORADO.EDU.

10.1021/jp9911752 CCC: $18.00
Published on Web 07/20/1999

with other tungsten oxide ions, is synthesized in a flowing afterglow apparatus by reacting tungsten hexacarbonyl vapor with an oxygen anion in a helium buffer gas downstream from a microwave discharge ion source. Typical WO_2^- currents are 5−10 pA and, in room temperature experiments, the ions have a vibrational temperature of 300 K following collisional relaxation. The spectrum was also collected under liquid nitrogen cooled flow tube conditions, lowering the vibrational temperature to approximately 200 K. Upon extraction from the flow tube, the ions are accelerated to 735 eV and mass-selected as they transverse a Wien velocity filter. After mass selection, the ions are decelerated to 38 eV prior to entering the laser interaction region. The ion beam is crossed with the 364 nm output of an argon ion laser in a buildup cavity with approximately 100 W of circulating power, as described previously.[13] Photodetached electrons are energy analyzed with a resolution of about 10 meV by using a hemispherical energy analyzer and detected by a position sensitive detector. Thus, the photoelectron spectra show the number of electrons detected as a function of the electron binding energy, determined by the difference between the laser photon energy (3.408 eV) and the electron kinetic energy.

The absolute energy scale is calibrated by the position of the $^3P_2 \leftarrow {}^2P_{3/2}$ transition in the O^- spectrum.[14] A small energy compression factor (<1%) is also applied. This factor is determined by the comparison of the peak positions in the spectrum of the tungsten ion (W^-) with the known transitions in tungsten atom.[15]

Spectra have been recorded at three different laser polarization angles. By rotating a half-wave plate situated in the laser beam path, spectra can be collected with the laser polarization plane 0° (parallel), 54.7° (magic angle), and 90° (perpendicular) relative to the electron detection axis. The asymmetry parameters (β) have been obtained by using the expression

$$\beta = \frac{I_0 - I_{90}}{\frac{1}{2}I_0 + I_{90}} \quad (1)$$

where I_0 and I_{90} are the peak intensities taken at 0° and 90°, respectively.[16]

Ab initio calculations of the ground electronic state of WO_2^-, as well as the first four electronic states of WO_2, were performed using the GAUSSIAN 94 suite of programs.[17] The calculations employed the density functional theory BP86 method and the LanL2DZ effective core potential/basis set for tungsten and the D95 basis set for oxygen (method 1). For comparison purposes we also carried out the calculations by using the more reliable B3LYP method, using the same ECP/basis set for tungsten, and the 6-31+G* basis set for oxygen (method 2). Because both methods give very similar results, only the values obtained from method 1 are included in the text and used for the simulations. The values obtained by using method 2, however, are included in the tables. Optimized geometries were obtained without any constraints in the C_{2v} subspace, and force constants were calculated to establish the true minima characteristics of the stationary points. The geometries, frequencies, and normal modes obtained as a result of these calculations were used to compute the Franck−Condon intensities by using a slightly modified version of the program CDECK.[18,19] These results in turn are used to generate a simulation of the photoelectron spectrum by convoluting the calculated Franck−Condon transitions with a Gaussian function (fwhm = 10 meV). This simulation aids in the assignment of the features in the experimental spectrum.

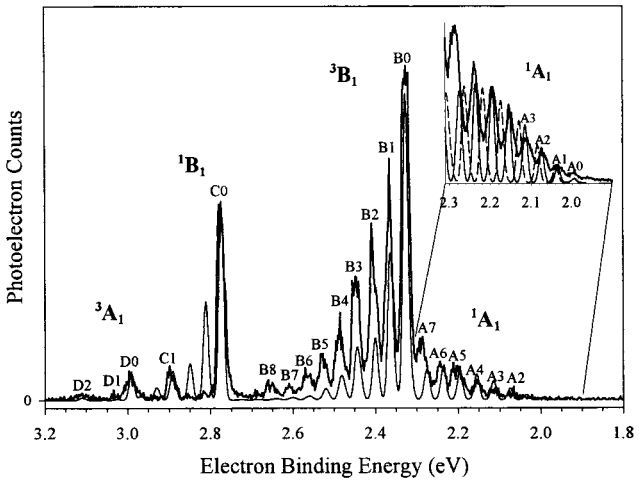

Figure 1. Photoelectron spectrum (364 nm) of WO_2^- taken at 200 K showing four different electronic states of WO_2. The simulated spectrum using method 1 is shown with a thin line. An expanded view of the $^1A_1$ region showing the simulated spectrum using theoretical frequencies (dashed line) and experimental frequencies (solid thin line) is shown in the inset; see text for details. The $^1B_1$ and $^3A_1$ assignments are tentative; see text for details.

Results and Analysis

The photoelectron spectrum of WO_2^- recorded at the magic angle is displayed in Figure 1. This spectrum was recorded with the flow tube cooled to approximately 200 K, as opposed to the 300 K obtained under room-temperature conditions. Upon cooling, the feature labeled A7 became narrower and less intense. The decrease in width and intensity is attributed to a hot band. The same spectrum also was recorded at two additional laser polarization angles, 0° and 90°; these spectra are not shown in this paper.

Figure 1 is composed of resolved, vibrational progressions in four different electronic states in the neutral molecule: the ground state and three excited electronic states. These are the states that are accessible with the 3.408 eV photon energy. The labeling of these electronic states is discussed in detail below. The band with peaks labeled A0−A7 is assigned as the neutral ground state. Peaks in the progressions labeled B, C, and D are transitions to various vibrational levels in three different excited electronic states. Each of the peaks in the spectrum was fit to a Gaussian function in order to obtain the energy position. These energy positions have been used to determine the electron affinity (EA) and to calculate the vibrational frequencies of the active modes within each individual electronic state, all of which are listed in Table 1, including the assignment for each peak in the spectrum. Two of the modes, the symmetric stretch (ν_1) and the bend (ν_2), are totally symmetric and could be present in the photoelectron spectrum.

The band assigned to the ground $^1A_1$ electronic state of WO_2 consists of a large number of vibrational transitions. The highest intensity feature within this state occurs at an energy corresponding to a transition with several quanta of vibrational excitation, suggesting a significant change in the geometry between the anion and neutral molecule. Table 2 shows that there is a large decrease in the O−W−O angle and the W−O bond length when going from the anion ground state to the neutral ground $^1A_1$ electronic state. As a result, the Franck−Condon factor for the $^1A_1$ ($\nu = 0$) ← $^2B_1$ ($\nu' = 0$) transition should be small, which makes it difficult to obtain an accurate value for the electron affinity. The inset of Figure 1 shows an expanded view of the low-energy portion of the photoelectron

TABLE 1: Experimental Peak Positions and Assignments of Features in the WO_2^- Photoelectron Spectrum[a]

				term energies (eV)	
neutral state	peak label	assignment[b]	peak position (eV)	exp[b]	calc[c]
$1A_1$	A0	2_0^k	1.998(10)	0.040*k*	
	A1	2_0^{k+1}	2.037		
	A2	2_0^{k+2}	2.073		
	A3	2_0^{k+3}	2.113		
	A4	2_0^{k+4}	2.153		
	A5	2_0^{k+5}	2.196		
	A6	2_0^{k+6}	2.239		
	A7	2_0^{k+7}	2.288		
$^3B_1$	B0	0−0	2.325(6)	0.327(6) + 0.040*k*	0.221 (0.216)
	B1	2_0^1	2.366		
	B2	2_0^2	2.405		
	B3	2_0^3, 1_0^1	2.446		
	B4	2_0^4, $2_0^1 1_0^1$	2.486		
	B5	2_0^5, $2_0^2 1_0^1$	2.525		
	B6	2_0^6, $2_0^3 1_0^1$,1_0^2	2.563		
	B7	2_0^7, $2_0^4 1_0^1$, $2_0^1 1_0^2$	2.602		
	B8	?	2.653		
$^1B_1$[d]	C0	0−0	2.774(6)	0.776(6) + 0.040*k*	0.698 (0.674)
	C1	1_0^1	2.894		
$^3A_1$[d]	D0	0−0	2.991(8)	0.993(7) + 0.040*k*	0.726 (0.645)
	D1	2_0^1	3.033		
	D2	1_0^1	3.108		

[a] Energies from the calculations are presented for comparison. Error bars are in. [b] By comparing the experimental spectrum with the Franck−Condon probabilities for the 0−0 transition we conclude that *k* can be 0, 1, or 2. See text for details. [c] Results obtained by using BP86/LanL2DZ. Values in parentheses are results using the B3LYP method and LanL2DZ ECP/basis set for tungsten and the 6-31+G* basis set for oxygen. Values do not include zero point energy corrections. [d] Tentative assignment. See text for details.

TABLE 2: Geometries of the Anion and Neutral Species Calculated Using BP86/LanL2DZ (Method 1)[a]

state	α (deg)	*R* (Å)	$\|\Delta\alpha\|$ (deg)	$\|\Delta R\|$ (Å)
		Anion		
$^2B_1$	116.44	1.76		
	(117.93)	(1.74)		
		Neutral		
$^1A_1$	103.79	1.72	12.65	0.04
	(104.75)	(1.69)	(13.19)	(0.05)
$^3B_1$	112.27	1.74	4.17	0.02
	(113.71)	(1.72)	(4.22)	(0.025)
$^1B_1$	112.06	1.74	4.38	0.02
	(113.62)	(1.72)	(4.31)	(0.024)
$^3A_1$	117.62	1.75	1.18	0.01
	(118.50)	(1.72)	(0.57)	(0.02)

[a] α is the O−W−O angle and *R* is the W−O bond distance. B3LYP/LanL2DZ/6-31+G* (Method 2) results in parentheses.

TABLE 3: Experimental and Calculated Frequencies[a]

	ν_1 (symmetric stretch)		ν_2 (bend)	
state	exp	calc[b]	exp	calc[b]
$^1A_1$		1014 (1071)	325(15)	361 (373)
$^3B_1$	995(25)	963 (1019)	320(15)	300 (311)
$^1B_1$[c]	970(15)	963 (1017)		302 (313)
$^3A_1$[c]	945(25)	952 (1011)	340(20)	276 (289)

[a] All values are in wave numbers (not scaled). Error bars are in parentheses. [b] Results of calculations using BP86/LanL2DZ. Values in parentheses are results using the B3LYP method and LanL2DZ ECP/basis set for tungsten and the 6-31+G* basis set for oxygen. [c] Tentative assignment. See text for details.

spectrum to aid in the identification of the EA. It is clear that there are additional peaks to lower energy of A2 that can be attributed to transitions to the neutral ground electronic state. The lowest energy feature that could be assigned as a transition from the lowest level in the anion to a vibrational level in the neutral is located at an electron binding energy of 1.998(10) eV (A0), which, as discussed below, could be considered as an upper limit of the electron affinity. The origin of the first excited state ($^3B_1$) is easily observed in the photoelectron spectrum at an electron binding energy of 2.325(6) eV (B0). The next excited state, the C series, also has a high-intensity 0−0 transition at 2.774(6) eV (C0). Finally, the origin of the third excited state, the D series, is well established at 2.991(8) eV (D0). The term energies obtained from these values agree very well with the calculated values, as can be seen in Table 1. The prominence of the 0−0 transition in the excited electronic states suggests that the geometry change between the anion and neutral is smaller than that for the ground state (Table 2).

In addition to the electron affinity and origin transitions, vibrational frequencies also have been extracted from the photoelectron spectrum (Table 3). In the ground electronic state the lowest vibrational frequency (the bending motion, ν_2) is measured to be 325(15) cm^{-1}, compared to the calculated value of 361 cm^{-1}. The frequency of the symmetric stretching vibration (ν_1) is difficult to measure in this electronic state because there is overlap with features corresponding to several quanta of excitation in the bending motion. Calculations predict a stretching frequency of 1014 cm^{-1}. The Franck−Condon calculations reveal that there is more intensity in the bending vibrational transitions than in the stretching mode, thus favoring the observation of ν_2. There have been several infrared matrix studies performed from which a value of ν_1 was determined. Andrews and co-workers[11] utilized infrared matrix spectroscopy to determine $\nu_1 = 978$ cm^{-1} after reacting laser-ablated tungsten with O_2 in an Ar matrix. Similarly, Green and Ervin[10] isolated WO_2 in a Kr matrix measuring a symmetric frequency of 975.5 cm^{-1} and Weltner et al.[12] reported $\nu_1 = 992$ cm^{-1} via Ne matrix studies.

The bending frequency in the $^3B_1$ state is close to that measured in the ground electronic state at 320(15) cm^{-1}, as compared to the calculated value of 300 cm^{-1}. This agrees well with the only other experimental value, 300 cm^{-1}, measured in an early infrared matrix study.[12] Again, it is difficult to measure an accurate frequency for ν_1 due to overlap with high quanta of ν_2. Upon closer examination, however, it appears that peak

B3 is broader than peaks B0, B1, and B2, possibly because of the overlap between two different vibrational transitions ($3\nu_2$ and $1\nu_1$) at 995(25) cm^{-1}, which cannot be resolved at the level provided by our spectrometer. This agrees well with our calculations, which give a value of 963 cm^{-1} and another theoretical value of 993 cm^{-1}.[11] Finally, it is difficult to determine whether peak B8 is part of the $^1A_1$ or $^3B_1$ electronic state progression. The spacing between it and B7 (410 cm^{-1}) is much larger than the other vibrational spacings. At this point, we do not attempt to assign this feature.

Within each of the two higher excited electronic states, only a few features are observed. Two clear features are seen within the second excited state, C0 and C1, which are separated by 970(15) cm^{-1}. We assign C0 to the 0−0 transition and C1 to one quantum of vibration in the symmetric stretch because ab initio calculations predict $\nu_1 = 963$ cm^{-1}. There is also a small peak located between C0 and C1 (not labeled) that can be attributed to the bending vibration, calculated to be 302 cm^{-1}. A similar pattern is observed within the third excited electronic state where features D0 and D2 are separated by 945(25) cm^{-1}, which we assign as the ν_1 frequency. This measured value agrees well with 952 cm^{-1} from the calculations. Peak D1 is assigned as one quantum of bending vibration at 340(20) cm^{-1}; this is in comparison to the calculated value of 276 cm^{-1}. All experimental and calculated frequencies are listed in Table 3.

Also displayed in Figure 1 is a simulation (thin line) of the photoelectron spectrum. The simulation is generated by implementing a series of programs that calculate the normal mode displacements and the Franck−Condon factors. A slightly modified version of the program CDECK,[18] which utilizes the geometries, normal modes, and force constants from the GAUSSIAN 94 output file, is employed to calculate the normal mode displacements. These results are then used to calculate Franck−Condon factors for transitions from the ground vibrational state of the anion (and therefore excluding hot bands) to various vibrational levels in the neutral electronic states. Finally, all of the peaks are convoluted with a 10 meV fwhm Gaussian function to produce the simulated spectrum. It is important to note that all of the frequencies are treated as harmonic frequencies when generating the spectrum.

As discussed above, the measured bending frequency for the ground $^1A_1$ electronic state is approximately 40 cm^{-1} smaller than the calculated value; therefore, a simulation using the theoretical values for the frequencies does not match the ground state spectrum, as illustrated by the dashed line in the inset of Figure 1. If, instead, the measured bending frequency is used to generate the simulation, then the experimental spectrum is well reproduced (thin solid line). By matching the most intense peak of the spectrum and the simulation, the predicted 0−0 transition in the simulation overlaps with peak A0, suggesting that this peak could be assigned as the EA of WO_2. However, we cannot rule out the possibility that we could be in error by a few quanta in ν_2. This could be due to errors in the calculation of the geometry changes between the anion and the neutral ground state that affects the Franck−Condon progression. Simulations based on ab initio calculations using method 2 (not shown) are consistent with peak A0 as the 0−0 transition, which suggests that in the worst case scenario we could be off by one but not more than two quanta in ν_2. A careful examination of the inset in Figure 1 shows what seems to be a shallow peak at a lower electron binding energy than peak A0, which could be interpreted in principle as part of the ν_2 progression (the A series of peaks). This peak could also be a hot band since it does not appear to follow the intensity pattern of the A progression of peaks and it seems to be separated from A0 by a smaller distance than the other peaks in the progression. This is consistent with the smaller ν_2 frequency (241 cm^{-1} by using method 1, not scaled) found for the anion. However, the signal in this part of the spectra is very low and we cannot unequivocally rule out the possibility that this peak is not part of the ν_2 progression of peaks. Due to these reasons, the EA of WO_2 can be reported as 1.998(10) − 0.040*k* eV, where $k = 0$, 1, or 2 depending on the number of ν_2 quanta A0 is away from the true EA.

TABLE 4: Experimental Origin Transitions and Asymmetry Parameters (β)[a]

transition	energy (eV)	β[b]
$^1A_1$ ($\nu' = 0$) ← $^2B_1$ ($\nu'' = 0$)	≤1.998(10)[c]	0.5
$^3B_1$ ($\nu' = 0$) ← $^2B_1$ ($\nu'' = 0$)	2.325(6)	1.3
$^1B_1$[d] ($\nu' = 0$) ← $^2B_1$ ($\nu'' = 0$)	2.774(6)	1.4
$^3A_1$[d] ($\nu' = 0$) ← $^2B_1$ ($\nu'' = 0$)	2.991(8)	0.8

[a] Error bars are in parentheses. [b] Asymmetry parameters are for the origin peak except in the ground $^1A_1$ electronic state where the peak at 2.239 eV (A6) was used. Error bars are estimated to be 0.1. [c] Upper limit of the electron affinity. [d] Tentative assignment. See text for details.

For the first excited electronic state, the experimental spectrum can be well represented by a simulation based solely on the ab initio results. However, the simulation does not accurately reproduce the experimental spectrum of the second excited electronic state. A progression that can be attributed to several quanta of bending vibration is not observed experimentally, although the simulation suggests that there is a significant amount of intensity in these transitions, as illustrated in Figure 1. Last, there is some discrepancy between the intensities in the experimental and theoretical spectrum of the third excited electronic state (D series). The main difference is the intensity of peak D1 (ν_2) relative to that of D0, as it is larger in the experimental spectrum than predicted by theory.

The spectra recorded at 0° and 90° reveal that the detachment is more efficient at 0° laser polarization for all the features in the spectrum. As a result, the asymmetry parameter, β, for each peak is positive. Upon closer examination, more information can be gained from the exact values of the β parameters (Table 4). The value of β is similar for the ground electronic state and the third excited electronic state, 0.5 and 0.8, respectively. In addition, the first and second excited electronic states have essentially the same value of β, 1.3 and 1.4, respectively. These asymmetry parameters can be useful in assigning the electronic states, as will be discussed below. The values of β along with the energies of the peaks used are shown in Table 4.

To establish the electronic structure of the anion and the neutral obtained upon detachment, a molecular orbital diagram can be constructed for WO_2 from the orbitals of WO and oxygen. The diagram shown in Figure 2 is similar to that used previously in the study of MoO and CrO.[20,21] The electronic configuration used for WO is identical to that of CrO and MoO since, as shown by Nelin and Bauschlicher,[22] all these species have a $^5\Pi$ ground state. Only those orbitals involved in the formation of the new bond or in the photodetachment process have been included in Figure 2. The new OW−O bond is formed by the interaction between the degenerate δ orbitals of WO and two of the p orbitals (pσ and pπ) of oxygen, forming a new σ and π bond, respectively. As a result, the degeneracy of the δ orbitals is lifted since the newly formed WO_2 molecule has C_{2v} symmetry. In addition, the third oxygen p orbital (pπ) can interact with one of the WO π orbitals that is aligned in the same plane. As a result of the perturbation, a new pair of π orbitals is formed. The remaining orthogonal π orbital and σ

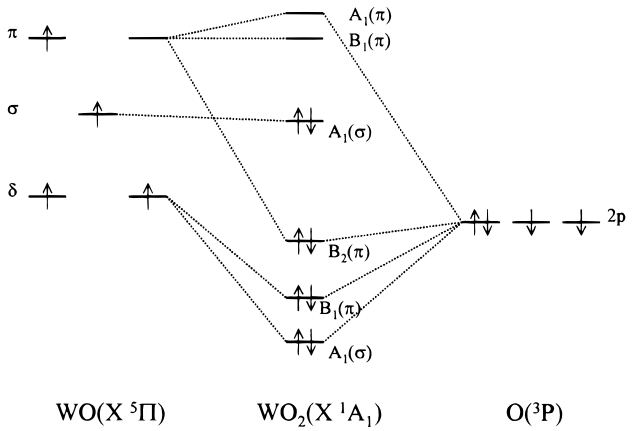

Figure 2. Molecular orbital correlation diagram for WO_2 ($^1A_1$) derived from WO and oxygen. Only those orbitals involved in the formation of the new bond or in the detachment process of WO_2^- to form the experimentally observed electronic states in the neutral are shown.

orbital of WO can be considered as unperturbed. The negative ion is formed by adding an additional electron to the lowest unoccupied B_1 (π) molecular orbital (LUMO), giving rise to a $^2B_1$ configuration. In general, our calculations agree with the qualitative picture. The order of the orbitals in WO_2 also agrees with what is shown in Figure 2, with the exception of the two lowest occupied molecular orbitals, which are very close in energy and switch positions in some of the excited electronic states.

Detaching an electron from these low-lying orbitals will give rise to a variety of electronic configurations for neutral WO_2. There are four states whose energies with respect to the anion are within our photon energy; they are illustrated in Figure 1 and are included in Table 1. Our theoretical results indicate that the lowest energy configuration for the neutral is the $^1A_1$ state (Table 1), which is formed when the electron in the single occupied molecular orbital (SOMO) (B_1) in the anion is detached (see Figure 2). This is in contrast to a recent paper[11] in which a triplet state is reported as the ground state by using the same theoretical level. Even though the exact electronic state for the triplet is not specified, by comparing geometries and frequencies, we conclude that the authors may have determined the $^3B_1$ state to be the ground state. Instead, we found the $^3B_1$ state as the first excited state of WO_2. This electronic state is formed by the detachment of the β electron from the A_1 orbital (SOMO-1) of the anion, leaving two α electrons in the two highest energy orbitals, A_1 and B_1 (see Figure 2). If instead the α electron from the SOMO-1 orbital in the anion is detached, a singlet state ($^1B_1$) is formed which, as shown in Table 1, is the second excited state of WO_2.

The last state predicted by the calculations to be observed in the 364 nm photoelectron spectrum of WO_2^- corresponds to a more complicated process. This $^3A_1$ state involves photodetachment of the β electron from the SOMO-1 (A_1) orbital of the anion, as in the formation of the $^3B_1$ state, and promotion of the α electron from the SOMO (B_1) to the LUMO (A_1).

It is interesting to note that the calculations agree well with the experimental spectrum in many areas. All of the electronic states of WO_2 that are predicted to lie within the 3.408 eV of available energy are observed in the photoelectron spectrum. The separations between the different excited electronic states with respect to the ground state (term energies) are very well estimated by the calculations considering the method and basis set used (Table 1). Furthermore, the geometries are predicted correctly for the ground and first excited electronic states, as revealed by the agreement between the experimental and the simulated spectra. However, as discussed above, the simulations are not as reliable for the second and third excited electronic states, which suggests that the geometries are not well determined by the calculations in these states. Last, the frequencies are in very good agreement with the values obtained from the spectrum with the exception of the bending vibration in the ground electronic state where the values differ by approximately 40 cm^{-1}.

The assignment of the two highest electronic states is not straightforward. On one hand, the relative intensities of the different states agree with the assignments of the electronic states. It has been observed in the photoelectron spectra of metal and metal oxide anions that the transitions involving the detachment of an electron from a σ orbital dominate the spectra.[20,21] This seems not to be an exception for WO_2^- where the two most intense peaks in the spectrum may correspond to the formation of the $^3B_1$ and $^1B_1$ states by detachment of the β or α electron of the σ orbital (SOMO-1) of the anion, respectively. However, if this is the case, the $^1B_1$ state should exhibit the same progression of peaks as the $^3B_1$ state. As shown above, this is observed in the simulation but not in the spectrum. For this reason we conclude that the assignment of the C series of peaks to the $^1B_1$ state should be viewed as tentative. In addition, the low intensities of the features assigned to the $^3A_1$ state are consistent with a two-electron process involved in the formation of this electronic state, as discussed above, although the disagreement between the simulation and the spectra suggests that the assignment of this state to the D series of peaks should also be considered tentative. On the other hand, the assignment of the $^1B_1$ and the $^3A_1$ states to the C and D series of peaks, respectively, is supported by the asymmetry parameters (Table 4). The $^3B_1$ and $^1B_1$ electronic states have similar values for β, indicating that the detached electron originates from the same type of orbital. In this case, a value of $\beta \approx 2$ indicates that the electron was detached from a σ orbital, as predicted by the calculations for these states. The $^3A_1$ state shows an asymmetry parameter similar to the $^1A_1$ state, but we think this is fortuitous. In the case of $^3A_1$, despite the fact that the detached electron comes from a σ orbital (as in the formation of the $^3B_1$ state) a second electron is promoted from a π orbital to a higher energy orbital, and the asymmetry parameter will depend on both processes. The β parameter for the $^1A_1$ state is intermediate between a σ orbital detachment and an isotropic distribution, indicating that some d orbital character is present in the orbital.

Conclusions

The 364 nm negative ion photoelectron spectrum of WO_2^- has been described. The spectrum reveals that four different electronic states are accessed in the neutral molecule following the detachment of an electron. The spectrum shows a great deal of vibrational structure from which the vibrational frequencies of the bending and/or symmetric stretching vibrations have been measured. The electron affinity has been determined to be $1.998(10) - 0.040k$ eV, where $k = 0$, 1, or 2. The origins of the three excited electronic states were also obtained. Theoretical calculations using the BP86 method and the LanL2DZ ECP/ basis set have been carried out to determine the geometries, energies, and frequencies of the anion and neutral molecules. Most of these results agree very well with the experimental measurements. The results were utilized to generate a simulation of the experimental spectrum. The simulation and the results of the calculations aid in the assignment of the electronic states and the vibrational frequencies.

For the ground ($^1A_1$) and the first excited ($^3B_1$) electronic states the excellent agreement between the spectrum and the simulation indicates that the changes in geometries upon detachment are well predicted by the theoretical method. These results are surprising considering the simplicity of the theoretical model. In addition, polarization studies enable the determination of the asymmetry parameters for each state, which further confirm the assignments of the electronic states. This study is in contrast to previous studies that suggest that the ground state is a triplet state. For the two highest observed electronic states (C and D series of peaks) the assignment of the electronic structure cannot be determined unequivocally. Evidence from the intensities of the 0−0 peaks, the asymmetry parameters, and theoretical results suggest that they may be $^1B_1$ and $^3A_1$ states, respectively.

Acknowledgment. This work was carried out as part of the undergraduate physical chemistry laboratory course at the University of Colorado. Students participating in the research were Scott Lynn, Heather Shaver, and Carolina Vong. Funding was provided by National Science Foundation Grants CHE97-03486 and PHY95-12150.

References and Notes

(1) Jones, F. H.; Egdell, R. G.; Brown, A.; Wondre, F. R. *Surf. Sci.* **1997**, *374*, 80−94.

(2) Gulino, A.; Parker, S.; Jones, F. H.; Egdell, R. G. *J. Chem. Soc., Faraday Trans.* **1996**, *92*, 2137−2141.

(3) Bolzan, A. A.; Kennedy, B. J.; Howard, C. J. *Aust. J. Chem.* **1995**, *48*, 1473−1477.

(4) Katrib, A.; Hemming, F.; Wehrer, P.; Hilaire, L.; Maire, G. *J. Electron Spectrosc.* **1995**, *76*, 195−200.

(5) Gesheva, K. A.; Gogova, D. S. *J. Phys. IV* **1993**, *3*, 475−483.

(6) Sheldon, R. A.; Kochi, J. K. *Metal Catalyzed Oxidants of Organic Compounds*; Academic Press: New York, 1981.

(7) Conte, V.; Di Furia, F.; Moro, S. *J. Phys. Org. Chem.* **1996**, *9*, 329−336.

(8) Almond, M. J.; Crayston, J. A.; Downs, A. J.; Poliakoff, M.; Turner, J. J. *Inorg. Chem.* **1986**, *25*, 19−25.

(9) Almond, M. J.; Downs, A. J. *J. Chem. Soc., Dalton Trans.* **1988**, 809−817.

(10) Green, D. W.; Ervin, K. M. *J. Mol. Spectrosc.* **1981**, *89*, 145−158.

(11) Bare, W. D.; Souter, P. F.; Andrews, L. *J. Phys. Chem.* **1998**, *102*, 2, 8279−8286.

(12) Weltner, J. W.; McLeod, J. D. *J. Mol. Spectrosc.* **1965**, *17*, 276−299.

(13) Ervin, K. M.; Lineberger, W. C. *Photoelectron Spectroscopy of Negative Ions*; Adams, N. G., Babcock, L. M., Eds.; JAI Press: Greenwich, CT, 1992; Vol. 1, p 121.

(14) Neumark, D. M.; Lykke, K. R.; Andersen, T.; Lineberger, W. C. *Phys. Rev. A* **1985**, *32*, 1890−1892.

(15) Moore, C. E. *Atomic Energy Levels*; U.S. GPO Circular No. 467; U.S. GPO: Washington, 1952.

(16) Cooper, J.; Zare, R. N. *J. Chem. Phys.* **1968**, *48*, 942−943.

(17) Frisch, M. J.; Trucks, G. W.; Schlegal, H. B.; Gill, P. M. W.; Johnson, B. G.; Robb, M. A.; Cheeseman, J. R.; Kieth, T.; Petersson, G. A.; Montgomery, J. A.; Raghavachari, K.; Al-Laham, M. A.; Zakrewski, V. G.; Ortiz, J. V.; Foresman, J. B.; Cioslowski, J.; Stefanov, B. B.; Nanayakkara, A.; Challacombe, M.; Peng, C. Y.; Ayala, P. Y.; Chen, W.; Wong, M. W.; Andres, J. L.; Replogle, E. S.; Gomperts, R.; Martin, R. L.; Fox, D. J.; Binkley, J. S.; Defrees, D. J.; Baker, J.; Stewart, J. P.; Head-Gordon, M.; Gonzalez, C.; Pople, J. A. *Gaussian 94, Rev. E.1*; Gaussian, Inc.: Pittsburgh, PA, 1995.

(18) Chen, P. *Unimolecular and Bimolecular Reaction Dynamics*; Ng, C. Y., Baer, T., Powis, I., Eds.; John Wiley & Sons: New York, 1994.

(19) We thank Peter Chen and Cameron Logan for providing us with a copy of their CDECK program.

(20) Gunion, R. F.; Dixon-Warren, S.; Lineberger, W. C.; Morse, M. D. *J. Chem. Phys.* **1996**, *104*, 1765−1773.

(21) Wenthold, P. G.; Gunion, R. F.; Lineberger, W. C. *Chem. Phys. Lett.* **1996**, *258*, 101−106.

(22) Nelin, C. J.; Bauschlicher, C. W., Jr. *Chem. Phys. Lett.* **1985**, *118*, 221−225.